Molecular assessment of surgical-resection margins of gastric cancer by mass-spectrometric imaging

Livia S. Eberlin[a], Robert J. Tibshirani[b], Jialing Zhang[a,c], Teri A. Longacre[d], Gerald J. Berry[d], David B. Bingham[d], Jeffrey A. Norton[e], Richard N. Zare[a,1], and George A. Poultsides[e]

[a]Department of Chemistry, Stanford University, Stanford, CA 94305-5080; [b]Departments of Health Research and Policy and of Statistics, Stanford University, Stanford, CA 94305-4065; [c]Department of Chemistry, Peking University, Beijing 100871, China; [d]Department of Pathology, Stanford University, Stanford, CA 94305-5324; and [e]Department of Surgery, Stanford University, Stanford, CA 94305-5641

Contributed by Richard N. Zare, January 7, 2014 (sent for review November 11, 2013)

Surgical resection is the main curative option for gastrointestinal cancers. The extent of cancer resection is commonly assessed during surgery by pathologic evaluation of (frozen sections of) the tissue at the resected specimen margin(s) to verify whether cancer is present. We compare this method to an alternative procedure, desorption electrospray ionization mass spectrometric imaging (DESI-MSI), for 62 banked human cancerous and normal gastric-tissue samples. In DESI-MSI, microdroplets strike the tissue sample, the resulting splash enters a mass spectrometer, and a statistical analysis, here, the Lasso method (which stands for least absolute shrinkage and selection operator and which is a multiclass logistic regression with L1 penalty), is applied to classify tissues based on the molecular information obtained directly from DESI-MSI. The methodology developed with 28 frozen training samples of clear histopathologic diagnosis showed an overall accuracy value of 98% for the 12,480 pixels evaluated in cross-validation (CV), and 97% when a completely independent set of samples was tested. By applying an additional spatial smoothing technique, the accuracy for both CV and the independent set of samples was 99% compared with histological diagnoses. To test our method for clinical use, we applied it to a total of 21 tissue-margin samples prospectively obtained from nine gastric-cancer patients. The results obtained suggest that DESI-MSI/Lasso may be valuable for routine intraoperative assessment of the specimen margins during gastric-cancer surgery.

mass spectrometry imaging | biostatistics | surgical margins | intraoperative diagnosis

Gastric cancer is currently the second most common cause of cancer death worldwide after lung cancer (1). Surgical resection of gastrointestinal (GI) cancers remains the main treatment option for these diseases. It is well accepted that complete resection of the tumor is associated with an improved prognosis for most types of solid malignancies. Positive margins, defined as the presence of tumor cells at the resected specimen edge and/or in the resection bed, have been associated with increased local recurrence and decreased overall survival in many cancers (2). Margin-negative surgical resection has the greatest potential to offer prolonged disease-free and overall-survival benefit across the entire spectrum of GI cancers (2–5). The evaluation is commonly performed in a room close to the operating room, where the proximal and distal margins of the surgical specimen are frozen, sectioned, stained, and read by pathologists before completion of the operation. The results of the intraoperative pathologic evaluation of the margins are communicated to the surgeon and consequently guide the surgeon's subsequent actions. For example, in the case of positive margins, surgical resection is extended by removing additional tissue around the tumor, which commonly demands a second round of margin evaluation by pathology. However, because of freezing artifacts on tissue morphology, intraoperative frozen-section results are subjective and can be unreliable in up to 30% of patients undergoing resection of gastrointestinal cancers (6–8). Moreover, processing, staining, and evaluation of multiple frozen sections can take up to 1 h, a time frame that can be detrimental in surgical practice. We present an alternative procedure, based on ambient mass spectrometry (MS) (9–13), for developing faster and more accurate evaluations of tumor margins during surgery.

Our procedure uses desorption electrospray ionization mass spectrometric imaging (DESI-MSI) (14) in combination with the least absolute shrinkage and selection operator (Lasso) technique (15, 16). This work builds on the previous, successful use of DESI-MSI for brain-tumor diagnosis (17, 18). DESI-MSI allows 2D mapping of the sample in the ambient environment, without the need of extensive sample preparation, at a rate of about 0.5 s per pixel. Samples are bombarded with microdroplets that dissolve hundreds of lipids and metabolites. The splash forms secondary microdroplets that enter a mass spectrometer, providing a detailed chemical map of the distribution of molecules within the sample surface (19). Because mass spectrometry provides such a wealth of chemical information, this technique invites a statistical analysis. We report the use of the Lasso technique (15, 16) to classify tissue as cancer or normal and also to select those molecular features most indicative of the disease state.

Many of the selected molecular ions were identified by tandem and high-resolution mass spectrometry as complex phospholipids and small metabolites of biological relevance. Note, however, that this identification is not necessary for using DESI-MSI/Lasso as a diagnostic tool although it could provide important information about gastric-cancer biochemistry. We further tested our method prospectively on the proximal and distal specimen margins

Significance

Complete resection of a tumor is associated with an improved prognosis for most types of solid malignancies. In gastric-cancer surgery, surgical-margin evaluation is commonly performed intraoperatively by histopathologic evaluation of frozen sections. However, frozen-section results are subjective and can be unreliable in up to 30% of patients undergoing resection of gastrointestinal cancers. We used desorption electrospray ionization mass spectrometric imaging (DESI-MSI) and the statistical method of least absolute shrinkage and selection operator (Lasso) to classify tissue as cancer or normal based on molecular information obtained from tissue and also to select those mass-spectra features most indicative of disease state. The results obtained using margin samples from nine gastric-cancer operations suggest that DESI-MSI/Lasso may be a valuable tool for routine intraoperative assessment of surgical margins during gastric-cancer surgery.

Author contributions: L.S.E., R.J.T., R.N.Z., and G.A.P. designed research; L.S.E., R.J.T., J.Z., T.A.L., G.J.B., D.B.B., and G.A.P. performed research; L.S.E., R.J.T., and J.A.N. contributed new reagents/analytic tools; L.S.E., R.J.T., T.A.L., and G.A.P. analyzed data; and L.S.E., R.J.T., R.N.Z., and G.A.P. wrote the paper.

The authors declare no conflict of interest.

[1]To whom correspondence should be addressed. E-mail: zare@stanford.edu.

This article contains supporting information online at www.pnas.org/lookup/suppl/doi:10.1073/pnas.1400274111/-/DCSupplemental.

of nine gastric-cancer operations in direct comparison with margin assessment by frozen-section histopathology, and we demonstrate that this approach could be very valuable for clinical use.

Results

Molecular Imaging of Gastric Tissue. Negative ion mode DESI-MSI was performed on 62 banked human gastric samples, including normal and cancerous gastric tissue. For most of the samples analyzed, evaluation of the 2D DESI-MSI images revealed some heterogeneity within the sample, with discrete regions within the samples that presented three main distinct spectral profiles: gastric adenocarcinoma, normal epithelium (mucosa), and normal stroma (submucosa) tissue, which were later verified by pathologic evaluation of the same tissue sections using H&E staining (20).

Fig. S1 shows representative negative ion mode DESI mass spectra for sample GC727, a poorly differentiated gastric adenocarcinoma with areas of cancerous tissue, and an adjacent normal gastric tissue with regions of both normal epithelial and adjacent normal stroma tissue. Most of the ions detected in the mass spectra were identified as small metabolites related to energy production, free fatty acids, fatty acid dimers, and complex phospholipids. An overall evaluation of the mass-spectral profiles reveals a higher similarity between the spectra obtained for gastric cancer and normal epithelial tissue than gastric cancer and stroma tissue, which is expected given the fact that gastric adenocarcinomas start from the inner epithelial layer of the stomach. Nevertheless, strong differences in the relative abundances of various ions were found within the three distinct regions, which can be clearly seen in the selected DESI-MS ion images (Fig. 1).

Diagnostic Feature Selection and Identification. The large number of molecular features obtained from the combination of all pixels throughout all of the 62 banked samples analyzed makes data interpretation difficult and calls for the use of multivariate statistical techniques (21–23). Models generated using the Lasso are simpler and easier to interpret than those from other linear regression methods, as it yields "sparse" models, that is, models that involve only a subset of the variables/predictors (24). Using the training set of samples (28 frozen banked samples from 14 patients), the Lasso selected a total of 120 *m/z* values that are important in characterizing all three classes and yielded the lowest cross-validation errors (Fig. 2 and Table S1). From those 120 *m/z* values, 44 different *m/z* values were selected by the classifier as important features to characterize gastric cancer whereas 46 *m/z* values and 30 *m/z* values were found as important features to characterize normal epithelium and normal gastric stroma, respectively.

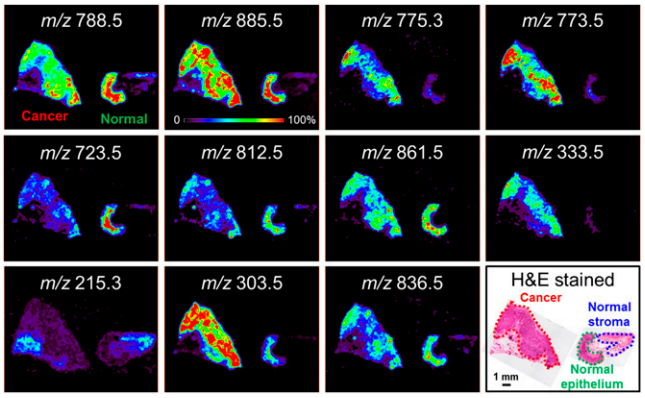

Fig. 1. Selected negative ion mode DESI-MS ion images of sample GC727. Higher relative abundances of the ions at *m/z* 775, *m/z* 773, *m/z* 303, *m/z* 747, *m/z* 797, and *m/z* 887 were observed in the region of cancer whereas higher relative abundances of the ions at *m/z* 788, *m/z* 723, *m/z* 812, and *m/z* 861 are observed in the region of normal gastric epithelial tissue, and higher relative abundances of the ions at *m/z* 737, *m/z* 818, *m/z* 215, and *m/z* 810 are observed in the regions with normal stromal tissue. Other ions, such as *m/z* 885, *m/z* 836, and *m/z* 281, show similar relative abundances throughout the cancerous and normal epithelial regions of the tissue sections. Shown is the optical image of the same tissue section subjected to H&E stain, with regions of cancer delineated in red, normal gastric epithelial tissue in green, and normal gastric stromal tissue in blue, as diagnosed by pathologic analysis.

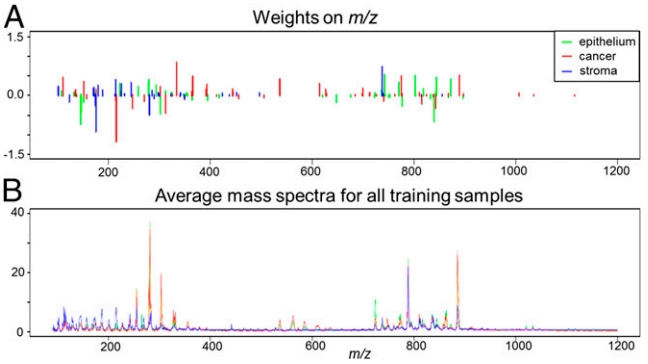

Fig. 2. The Lasso method yields a model with parsimonious sets of features for discriminating between gastric adenocarcinoma, normal epithelial tissue, and normal gastric stromal tissue. A mathematical weight for each statistically informative feature is calculated by the Lasso depending on the importance of the height (or ion abundance) of that peak in characterizing a certain class. Features that do not contribute to characterizing a class receive a weight of zero and are disregarded. An ion whose peak height, or abundance, is important for characterizing a certain class is given a positive weight whereas ions whose low abundances or absence are important receive a negative weight. The peak weights given by the Lasso to each of the selected mass-spectral features are shown in the mass spectra for each *m/z* value, with weights for each class displayed in its respective color (epithelium in green, cancer in red, and stroma in blue), as shown in *A*. The average mass spectra for each class for all pixels obtained for the training samples are shown in its respective color in *B*.

Many of the ions selected as statistically significant by the Lasso were tentatively identified as biologically relevant molecules (Table S2) using high mass resolution/high mass accuracy and tandem mass spectrometry analyses of tissue sections. For example, the species with *m/z* 723.3, which received a positive weight by the Lasso for characterizing normal epithelial tissue, was a doubly charged ion whose accurate mass and isotopic distribution matched that of the doubly deprotonated form of the cardiolipin CL(1′-[18:2/18:2],3′-[18:2/18:2]), with a mass error of +1.93 ppm. CLs are interesting complex phospholipids (PLs) found almost exclusively in the inner mitochondrial membrane of cells and are intimately involved in maintaining mitochondrial functionality, membrane integrity, and ultimately in energy production and metabolism (25). Remarkably, major abnormalities in CL content such as deficiency of this mature CL specie have been reported in cancer (25). Other important peaks that were given positive weight for the normal epithelial tissue class were identified as phospholipid (PL) species such as glycerophosphoethanolamine PE(36:1) at *m/z* 742.6, glycerophosphoserine PS(36:1) at *m/z* 788.5, and PS (38:1) at *m/z* 816.5, based on accurate mass measurements (mass errors of less than +1.60 ppm) and tandem MS experiments in comparison with literature on the fragmentation patterns of these lipid species (26–28). Note that isomerism of the double bonds in the fatty-acid (FA) chains of complex lipids complicates precise structural assignment, which is why FA chains are solely tentatively assigned. Besides PL species, small molecules related to energy and metabolism, such as *m/z* 145.2 and *m/z* 146.2, which were respectively tentatively assigned as the amino acids glutamine and glutamate, were selected by the Lasso as being statistically significant for the epithelial class with a negative weight, which indicates that a small relative abundance of these peaks in comparison with that detected in other classes is important for characterizing normal epithelial tissue. Interestingly, a peak at *m/z* 312.2 was selected by the Lasso as

important for characterizing both gastric cancer and normal epithelial tissue but with a positive weight for cancer and negative weight for normal tissue. High mass accuracy experiments revealed that the mass of this ion matched that of the deprotonated form of palmitoylglycine, an endogenous metabolite of fatty acids whose function has been related to the production of anti-inflammatory effects in tissue (29). Furthermore, a few other peaks that were given a positive weight for characterizing gastric cancer were identified as polyunsaturated fatty acids, such as docosatrienoic acid at *m/z* 333.3, as well as PLs such as PS(38:4) at *m/z* 810.5 and PI(38:3) at *m/z* 887.8. Indeed, many reports have described abnormal fatty-acid and PL composition in various types of adenocarcinomas (30, 31). In the case of stromal tissue, a negative weight was assigned to a peak at *m/z* 175.1, which was assigned as ascorbic acid, whereas positive weight was given to an ion at *m/z* 737.5, which was assigned as a chlorine adduct of the sphingolipid sphingomyelin(d16:1/18:0). Note, however, that, whereas chemical identification of the mass spectra features is not necessary for tissue diagnosis by DESI-MSI/Lasso, these results demonstrate that our method can clearly pinpoint important molecules that could be related to gastric-cancer biochemistry.

Statistical Approaches and Predictions. The Lasso yields a classifier that predicts whether a pixel belongs to a certain class based on the probability of it being assigned as cancer, normal epithelium, or normal stroma. Our training set consisted of 28 banked tissue samples from 14 different patients, which contained clearly demarcated areas of tissue diagnosed by pathologic examination, with regions delineated as cancer or normal gastric tissue. To test our model, which was built to classify on a per-pixel basis, we performed a 14-fold leave-one-patient-out cross-validation and evaluated the agreement between the prediction obtained by Lasso and the diagnosis of cancer, normal epithelium, or normal stroma obtained by histopathologic evaluation of the same frozen tissue section that was imaged by DESI-MSI and then subjected to H&E staining (see *SI Text* for additional explanation). When a total of the 12,480 pixels used as testing set were tested through cross-validation for the three classes, an overall agreement rate of 96.2% was achieved, as shown in Table 1. The cancer class showed the highest agreement (98.0%) with pathologic evaluation, followed by stroma class (96.1%) and epithelial tissue (93.4%). Because part of the disagreement occurs between stroma and epithelium classes that are both normal gastric tissue, we combined these two classes as one normal tissue class versus gastric-cancer class, which yields an overall agreement rate of 97.8%. In fact, discrimination between normal versus cancerous gastric tissue is the most important diagnostic information.

The classification results for each pixel are represented in a 2D space with cancer shown as red pixels, normal stroma as blue pixels, and normal epithelial tissue as green pixels, allowing a direct comparison with the optical image of the H&E stained tissue. For example, Fig. 3 *A* and *B* shows the DESI-MSI ion image for *m/z* 788.5, PS(36:1), and the classification results obtained for samples GC727, GC167, and GC737, respectively. The optical image of the H&E-stained section with pathologic diagnosis is shown in Fig. 3*C*. All of these samples contained regions of gastric cancer as well as adjacent tissue with regions of both normal epithelial and normal stroma tissue. In many cases, the discrepant pixels were spatially located at bordering regions with histological heterogeneity, which could account for the discrepancy with the overall diagnosis given by the pathologist. Note that pathologic assignment of regions within the training set of samples was performed in areas of clear diagnosis, in which the majority of the tissue consisted of one tissue class. Nevertheless, microscopic histological heterogeneity could still be present and be picked up by the Lasso classifier. For example, for sample GC167, a pixel localized in the edge between the large cancer region and a neighboring region, where cancer is invading surrounding stroma, was classified as stroma. In the adjacent tissue piece, few pixels in the border between epithelial tissue and stroma tissue were classified as stroma tissue.

Table 1. Prediction results for the 12,480 pixels analyzed in the training set of samples, in comparison with pathological analysis

	Predicted			
Pathology*	Cancer	Epithelium	Stroma	Agreement, %
Cancer	5,809	114	2	98.0
Epithelium	134	3,566	118	93.4
Stroma	25	82	2,630	96.1
				Overall: 96.2

	Cancer	Normal	Agreement, %
Cancer	5,809	116	98.0
Normal	159	6,396	97.6
			Overall: 97.8

	Presmoothing Predicted			
Pathology	Cancer	Epithelium	Stroma	Agreement, %
Cancer	5,895	30	0	99.5
Epithelium	85	3,657	76	95.8
Stroma	4	34	2,699	98.6
				Overall: 98.2

	Cancer	Normal	Agreement, %
Cancer	5,895	30	99.5
Normal	89	6,466	98.6
			Overall: 99.0

*Pathologic analysis was performed on the same frozen tissue section used for DESI-MSI that was H&E stained after MSI analysis.

An additional approach for classifying 2D images is to apply a spatial smoothing technique, which considers the statistical probability of the neighboring pixels to be in a certain class when

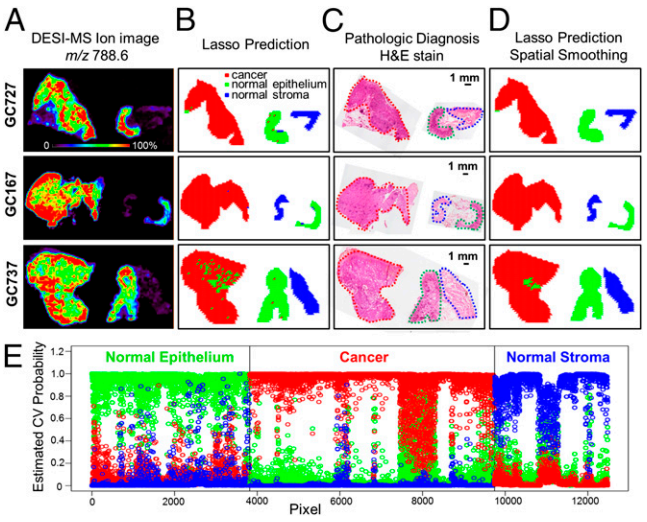

Fig. 3. DESI-MSI and Lasso prediction results obtained for samples GC727, GC167, and GC737. In *A*, negative ion mode DESI-MS ion images of *m/z* 788.6 are shown for each sample. Lasso prediction results are shown in *B* for each sample, with pixels predicted as cancer shown in red, as normal epithelium shown in green, and normal stroma shown in blue. In *C*, optical images of the H&E stained tissue sections are shown with the regions diagnosed by pathologists delineated in dots using the same color representation. Lasso prediction results with spatial smoothing are shown in *D* for each sample using the same color representation. In *E*, cross-validated class probability estimates (epithelium in green, cancer in red, and stroma in blue) are shown. Each vertical column depicts the three class probabilities for each pixel. The three panels (*Left*, *Center*, *Right*) indicate the true class of each pixel (displayed in arbitrary order).

classifying a central pixel. Fig. 3*D* show the results obtained for samples GC727, GC167, and GC737 after the presmoothing technique was applied, which shows full agreement with pathologic diagnosis. Overall, 99.0% accuracy with histological diagnosis was obtained for cross-validation when the spatial smoothing technique was applied (Table 1).

The classification system was built to allow a pixel to be classified in the one class for which the pixel has the highest probability of belonging. Fig. 3*E* shows a graph of the estimated cross-validation probabilities for each class for all of the 12,480 pixels tested in cross-validation, with the probabilities (0–1) of a certain pixel being classified as epithelium shown in green, cancer in red, and stroma in blue. Note that the great majority of pixels diagnosed as epithelium by pathologic examination have a probability greater than 0.80 of being classified as epithelium by the Lasso classifier. A similar trend is observed for pixels diagnosed by pathology as gastric cancer, with most of the second highest probabilities as epithelium, as it would be expected, and very low probabilities of stroma classification. In the case of pixels diagnosed as stroma, the probabilities are spread among the three classes, with still highest probably (>0.4) as stroma for the great majority of the pixels.

An approach to account for possible disagreements from low classification probabilities would be to establish a probability gap needed for class assignment; if the pixel does not meet that requirement, it would be placed in an unclassified "don't-know" category. This approach could be very important in clinical practice when one could choose to make a decision depending on the level of confidence that the classifier has in its prediction. To test this approach, we established a probability gap of 0.2, meaning that the pixel would be classified as a certain class only if the highest probability of belonging in one class would be at least 0.2 higher than the next highest probability. The results for this approach are reported in Table S3 for all pixels tested in cross-validation. As observed, 3.9% of the pixels fall into the don't-know category whereas the overall agreement rate increases to 98.4%. Fig. S2 shows the 2D results obtained for samples GC167, GC727, and GC737, in which the unclassified, don't-know pixels are displayed in gray.

Predictions for Validation Sets. We analyzed two independent sets of samples to test the performance of our classifier. The first set of samples consisted of 12 tissue samples with clear regions of cancer and normal adjacent tissue. Fig. S3 shows the results obtained for validation set sample GC962, in which clear agreement between histopathologic evaluation and DESI/Lasso results was obtained. The classification results obtained for the test set of the sample are shown in Table S4. Note that the majority of the discrepancies occurred between normal epithelium and normal stromal pixels, for which a small percentage of the pixels are misclassified as cancer. Overall, an agreement of 97.3% between pathologic diagnosis and classification results for cancer versus normal tissue was obtained for the total of 5,839 pixels evaluated in the validation set of samples. When spatial smoothing was applied, an overall agreement of 98.7% was achieved. The next test set included samples of difficult pathologic diagnosis or of high histological heterogeneity, such as cancer infiltrating normal stromal or epithelial tissue. For example, sample GC259 consisted of a tissue piece in which the top region had a high concentration of poorly cohesive (signet ring) carcinoma cells (~80% tumor cells), neighboring or within normal epithelial tissue. A few cancer cells also infiltrated the stromal region in the bottom of the tissue section. Fig. 4 shows the results obtained by DESI-MSI/Lasso for samples GC729 and GC259, two cases of extensive histological heterogeneity for which a high correlation was obtained by DESI-MSI/Lasso prediction and histopathologic diagnosis.

Surgical-Margin Evaluation. To further validate the DESI-MSI/Lasso classification system for surgical margin assessment, we analyzed 21 samples obtained from nine gastric-cancer operations

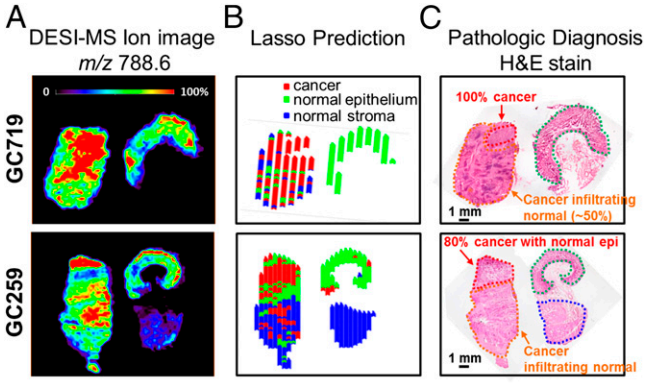

Fig. 4. DESI-MSI and Lasso prediction results obtained for samples GC719 and GC259. In *A*, negative ion mode DESI-MS ion images of *m/z* 788.6 are shown for each sample. Lasso prediction results are shown in *B*, with pixels predicted as cancer shown in red, as normal epithelium shown in green, and normal stroma shown in blue. In *C*, optical images of the H&E-stained tissue sections are shown with the regions diagnosed by pathology delineated using the same color representation.

that were performed at Stanford University Hospital. During the course of the operation, the resected tissue was taken from the operating room to the frozen-section room following standard clinical workflow for tumor-margin assessment. For most of the gastric-cancer surgeries, immediately adjacent sections of the proximal and the distal margins were obtained and analyzed by DESI-MSI/Lasso and compared with pathologic evaluation. Spatial smoothing was not applied for the margin samples as these could contain a fairly low amount of cancer (if present), which could be undesirably disregarded when considering the classification results of the normal neighboring pixels. Among the gastric-cancer surgeries, positive margins were diagnosed by pathology for the first proximal and/or distal margins in three surgical cases whereas negative margins were found for the remaining six cases.

We present the detailed results for two of the nine gastric-cancer surgeries in comparison with histopathology. Patient B had a complicated case of widely invasive poorly cohesive (signet ring) gastric carcinoma that was spreading toward the esophagus proximally and the duodenum distally. During surgical resection, both the proximal and distal margins were found to be positive by pathologic evaluation of frozen sections. The proximal margin was a small piece of esophageal tissue that contained small clusters of cancer cells invading the normal epithelial and stromal tissues. The distal margin consisted of duodenal tissue that also showed scattered cancerous cells invading throughout the tissue piece. A section of the proximal and distal margins was obtained for DESI-MSI. As surgery progressed, a second set of margins was obtained. The repeat distal margin was negative. The repeat esophageal (proximal) margin continued to be positive, with foci containing a high accumulation of cancer cells, in comparison with the first margin obtained. A serial section of the repeat esophageal margin only was also evaluated by DESI-MSI. The results obtained are presented in Fig. 5. As observed, the presence of cancer was detected in both the first distal and first proximal margins. In the distal margin, cancer was detected in a larger number of pixels than those diagnosed by histopathologic evaluation. In the case of esophageal margin, only a small region was detected as cancerous. Note that, for the repeat proximal margin section, many pixels were detected as cancer by DESI-MSI/Lasso, which is in agreement with what was observed by histopathologic evaluation. The surgeon proceeded to resect a third and final proximal margin, which was negative by frozen section (not evaluated by DESI-MSI).

Patient C was diagnosed with a poorly cohesive (signet ring) gastric adenocarcinoma. During surgical resection of the tumor

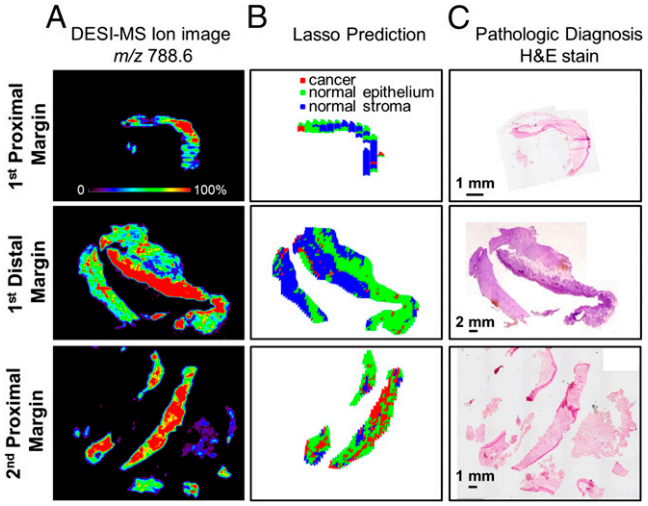

Fig. 5. DESI-MSI and Lasso prediction results obtained for gastric-cancer patient B. In *A*, negative ion mode DESI-MS ion images of *m/z* 788.6 are shown for cancer section, distal margin, and proximal margin. Lasso prediction results are shown in *B* for each sample, with pixels predicted as cancer shown in red, as normal epithelium shown in green, and normal stroma shown in blue. In *C*, the optical images of the H&E stained tissue sections diagnosed by pathology are shown.

margins, histological evaluation of both proximal (stomach) and distal (duodenum) margins was found to be quite challenging by frozen-section analysis. The first read by one pathologist diagnosed the proximal margin as negative for cancer whereas the distal margin was diagnosed as being positive for cancer. Nevertheless, when a second pathologist was called to read the same tissue sections, the conclusion was that both were negative for the presence of cancer. DESI-MSI was performed in adjacent sections of both the proximal and distal margins. After DESI-MSI, the same tissue section was stained and evaluated by two other pathologists. Evaluation of the H&E-stained margin sections by the first pathologist did not detect presence of cancer in any of the margin sections whereas evaluation by the second pathologist of the same tissue section was undefined for the distal margin, with doubts regarding the possible presence of poorly differentiated tumor, or a diagnosis of gastritis. The final agreement from detailed pathologic analysis was that both margins were negative for cancer. For both of the margin samples, classification by Lasso did not diagnose any of the pixels as being positive for cancer, as the entirety of both tissue sections was predicted as negative for cancer, mostly classified as normal epithelium and stroma tissue. This case is a powerful example of how DESI-MSI could assist as a complementary tool in surgical practice for margin assessment, especially in cases when frozen-section analysis is so difficult that disagreement in pathologic readings may occur.

Overall, close agreement with histopathology was achieved for all cases investigated. Full agreement was obtained for the 17 samples evaluated for gastric-cancer patients A, B, C, D, E, F, H, and J. The exceptions were for the distal margin of gastric-cancer patient F, the proximal margin of gastric-cancer patient G, and both distal and proximal margins of cancer patient H, for which a few pixels were detected as positive for cancer that were not confirmed by histopathology. For patient E, DESI-MSI/Lasso successfully predicted high-grade dysplasia (32) as positive for gastric cancer (Fig. S4). For patient A, a case of localized intestinal-type gastric adenocarcinoma, high agreement was achieved for proximal, distal, and cancer sections (Fig. S5). Detailed discussion and results for several of these cases are presented in *SI Text*.

Discussion

We have used the Lasso method to develop an automated system to classify tissue sections based on the molecular information obtained from DESI-MSI. Using different sets of training and validation samples, we showed that our method has high agreement with pathologic analysis on a per pixel basis, for banked tissue samples that had a definite pathologic diagnosis by frozen-section analysis. Using a set of validation samples with mixed features, we showed that, even in samples of complex morphology, such as regions with cancer infiltrating normal tissue or sparse foci of high grade dysplasia, the classification results obtained by our method were in close agreement with pathologic diagnosis. By developing spatial-smoothing techniques and setting statistical cutoff values, we provide statistical tools that could be valuable for clinical use.

Finally, by testing our method on complex margin samples obtained prospectively from gastrectomy cases, we demonstrated that DESI-MSI/Lasso could be a valuable combination to complement frozen-section analysis for margin assessment during surgery, especially in cases where frozen-section analysis is challenging and there is disagreement between pathologists. For this proof-of-concept study, we used 2D DESI-MSI for margin assessment so that a direct comparison could be done with histopathology of frozen sections with clear diagnosis. In a few cases, DESI-MSI/Lasso was able to identify cancerous regions that were missed on first pathologic examination but later confirmed. In practice, we expect DESI-MSI analysis to be performed in selected regions of diagnostic ambiguity, thereby enhancing intraoperative margin assessment by the pathologist. As DESI is performed in the ambient environment, no additional sample preparation is required. An additional benefit of using the Lasso method to generate the statistical models is that Lasso also allows for mass spectra feature selection, by which we were able to identify the molecules that are statistically significant for characterizing cancerous and noncancerous (epithelial or stromal) gastric tissue in conjunction with tandem and high mass accuracy/resolution mass-spectrometry studies. Ultimately, these molecules could provide new biological insights in gastric-cancer biochemistry. The findings described above provide evidence that the molecular information obtained by DESI-MSI/Lasso from tissue samples has the potential to transform the evaluation of surgical specimens. We believe the described methodology could be used in other GI cancers for which surgical-margin assessment is of critical importance.

Materials and Methods

Banked Human Gastric and Normal Gastric Tissues. Sixty-two frozen human tissue specimens including cancer and normal gastric tissue were obtained from the Stanford University Tissue Bank under approved Institutional Review Board (IRB) protocol. Samples were stored in a −80 °C freezer until sectioned. Tissue samples were sectioned at 15-μm-thick sections using a Leica CM1950 cryostat (Leica Mycrosystems Inc.). When samples of cancer and adjacent normal tissue were obtained from the same donor, the tissue sections were mounted onto the same glass slide adjacent to each other for analysis. After sectioning, the glass slides were stored in a −80 °C freezer. Before MS imaging, the glass slides were dried in a dessicator for ~15 min.

Prospective Evaluation of Gastrectomy Surgical Margins by DESI-MSI. Nine gastric-cancer patients scheduled to undergo cancer resection surgery at Stanford University Hospital were preoperatively consented for our study. Required IRB regulatory approvals were obtained. During gastric-cancer resection surgery, the proximal and distal margins of the gastrectomy specimen were subjected to frozen-section histopathologic evaluation, as routinely performed independently of our research. In parallel to the process of frozen section, adjacent 5- and 15-μm-thick tissue sections of each margin were obtained for DESI-MSI. For five of the nine patients, a sample of the tumor was obtained in addition to the proximal and distal margins. For one case in which positive margins were diagnosed during surgery, a second margin sample was also obtained for MS imaging. In total, 21 tissue samples were evaluated by DESI-MSI.

DESI-MSI. A laboratory-built DESI-MSI source coupled to an LTQ-Orbitrap XL mass spectrometer (Thermo Scientific) was used for tissue imaging. DESI-MSI was performed in the negative ion mode from *m/z* 90–1,200, using the linear ion trap as the mass analyzer. The spatial resolution of the imaging experiments was of 200 μm. The histologically compatible solvent system dimethylformamide:acetonitrile (DMF:ACN) 1:1 (vol/vol) was used for analysis (20), at a flow rate of 0.8 μL/min. The N_2 pressure was set to 175 psi. For ion identification, the Orbitrap analyzer was used for high mass resolution/accuracy measurements using the same tissue sections analyzed with the ion trap analyzer. Tandem MS analyses were performed using both the Orbitrap and the linear ion trap for mass analysis.

Histopathology. The same tissue sections of the banked tissue samples analyzed by DESI-MSI were subjected afterward to a standard H&E staining protocol. All of the samples used were frozen before sectioning, sectioned, and imaged by DESI-MSI, and then the same tissue section was fixed in methanol before staining with H&E (see *SI Text* for additional explanation). The tissue sections obtained from the 10 gastric-cancer surgeries, however, were serial to, but not the same sections used during surgery for surgical-margins assessment. Pathologic evaluation was performed by G.J.B., T.A.L., and D.B.B. using light microscopy. Regions of clear diagnosis of cancer, normal gastric epithelial tissue, and normal gastric stromal tissue were delineated in the glass slides when possible.

Statistical Analysis–Lasso Method. The Xcalibur raw data were converted to txt files for statistical analysis. The 2D raw data obtained by DESI-MSI were converted to text files and imported to R language for statistical analysis. The images were plotted in R, and a tool was developed to manually segment the regions of interest into different regions of clear pathologic diagnosis. Intensities of a total of 13,320 *m/z* values were recorded in each spectrum. To reduce complexity and account for small differences in registration between spectra, these values were averaged in nonoverlapping bins of six *m/z* values to yield a total of 2,220 features per spectrum. We randomly divided the patients into a training set (28 samples from 14 patients) and two test sets of samples (12 samples from 6 patients, and 22 samples from 11 patients). Within the training set, we applied the Lasso method (multiclass-logistic regression with L1 penalty) using the glmnet package in the CRAN R language library (33).

Models generated using the Lasso are simpler and easier to interpret than those from other linear-regression methods, as it yields sparse models, that is, models that involve only a subset of the variables/predictors (24). In our application, the Lasso method yields a model with parsimonious sets of features for discriminating between gastric adenocarcinoma, normal epithelial tissue, and normal gastric stromal tissue. A mathematical weight for each statistically informative feature is calculated by the Lasso depending on the importance that the mass-spectral feature has in characterizing a certain class. Because the features selected by the Lasso can occur at a valley or a shoulder of an actual mass-spectra peak, identification of the selected features was performed by characterizing the nearest mass-spectra peak to the statistically selected feature. Classification was done on a pixel-by-pixel basis into one of three classes: epithelium, cancer, or stromal. We used 14-fold cross-validation, leaving out one patient at a time, to select the Lasso tuning parameter and to assess the predictive accuracy within the training set. Then, the chosen model was applied to the test set of six patients and further samples. We also tried nearest-neighbor spatial smoothing of the predicted class probabilities, before the prediction of pixels in cross-validation and the test set. We also tried combining the epithelial and stroma classes into one normal class, and then training on just two classes— normal versus cancer. This approach produced similar results to the three-class training approach above, collapsing the predictions post hoc. Other prediction methods such as support vector machine and glmnet on principal component analysis were tested for classification. However, the Lasso method yielded better results than any other methods tested.

ACKNOWLEDGMENTS. We thank the Stanford University Tissue Bank for the services provided. This work was supported by the 2012 Stanford Hospital and Clinics Cancer Innovation Fund Award. L.S.E. is grateful to the Center of Molecular Analysis and Design for a postdoctoral fellowship. R.J.T. is supported by National Science Foundation Grant DMS-9971405 and National Institutes of Health Grant N01-HV-28183. J.Z. thanks the China Scholarship Council affiliated with the Ministry of Education of China (Grant 201206010110).

1. World Health Organization (2013) *Cancer (Fact Sheet No. 297)*. Available at http://www.who.int/mediacentre/factsheets/fs297/en/index.html.
2. Shoup M, Bouvet M, Farnell M (2012) Fluorescence-guided surgery allows for more complete resection of pancreatic cancer, resulting in longer disease-free survival compared with standard surgery in orthotopic mouse models discussion. *J Am Coll Surg* 215(1):135–136.
3. Han SS, et al. (2006) Analysis of long-term survivors after surgical resection for pancreatic cancer. *Pancreas* 32(3):271–275.
4. Conlon KC, Klimstra DS, Brennan MF (1996) Long-term survival after curative resection for pancreatic ductal adenocarcinoma: Clinicopathologic analysis of 5-year survivors. *Ann Surg* 223(3):273–279.
5. Zhang M, et al. (2012) Prognostic predictors of patients with carcinoma of the gastric cardia. *Hepatogastroenterology* 59(115):930–933.
6. Al-Ghnaniem R, et al. (2008) Strategy to reduce the risk of positive pancreatic resection margin at pancreatico-duodenectomy. *ANZ J Surg* 78(4):237–239.
7. Yamaguchi K, et al. (2005) Frozen section and permanent diagnoses of the bile duct margin in gallbladder and bile duct cancer. *HPB* 7(2):135–138.
8. Shen JG, et al. (2006) Intraoperative frozen section margin evaluation in gastric cancer of the cardia surgery. *Hepatogastroenterology* 53(72):976–978.
9. Seeley EH, Schwamborn K, Caprioli RM (2011) Imaging of intact tissue sections: Moving beyond the microscope. *J Biol Chem* 286(29):25459–25466.
10. Balog J, et al. (2013) Intraoperative tissue identification using rapid evaporative ionization mass spectrometry. *Sci Transl Med* 5(194):94ra93.
11. Dill AL, Eberlin LS, Ifa DR, Cooks RG (2011) Perspectives in imaging using mass spectrometry. *Chem Commun (Camb)* 47(10):2741–2746.
12. Harris GA, Galhena AS, Fernández FM (2011) Ambient sampling/ionization mass spectrometry: applications and current trends. *Anal Chem* 83(12):4508–4538.
13. Wu C, Dill AL, Eberlin LS, Cooks RG, Ifa DR (2013) Mass spectrometry imaging under ambient conditions. *Mass Spectrom Rev* 32(3):218–243.
14. Wiseman JM, Ifa DR, Song QY, Cooks RG (2006) Tissue imaging at atmospheric pressure using desorption electrospray ionization (DESI) mass spectrometry. *Angew Chem Int Ed Engl* 45(43):7188–7192.
15. Tibshirani R (1996) Regression shrinkage and selection via the Lasso. *J R Stat Soc B* 58(1):267–288.
16. Tibshirani R (1997) The lasso method for variable selection in the Cox model. *Stat Med* 16(4):385–395.
17. Eberlin LS, et al. (2013) Ambient mass spectrometry for the intraoperative molecular diagnosis of human brain tumors. *Proc Natl Acad Sci USA* 110(5):1611–1616.
18. Eberlin LS, et al. (2012) Classifying human brain tumors by lipid imaging with mass spectrometry. *Cancer Res* 72(3):645–654.
19. Costa AB, Cooks RG (2008) Simulated splashes: Elucidating the mechanism of desorption electrospray ionization mass spectrometry. *Chem Phys Lett* 464(1-3):1–8.
20. Eberlin LS, et al. (2011) Nondestructive, histologically compatible tissue imaging by desorption electrospray ionization mass spectrometry. *ChemBioChem* 12(14):2129–2132.
21. Alexandrov T (2012) MALDI imaging mass spectrometry: Statistical data analysis and current computational challenges. *BMC Bioinformatics* 13(Suppl 16):S11.
22. Dill AL, et al. (2010) Multivariate statistical differentiation of renal cell carcinomas based on lipidomic analysis by ambient ionization imaging mass spectrometry. *Anal Bioanal Chem* 398(7-8):2969–2978.
23. Pirro V, Eberlin LS, Oliveri P, Cooks RG (2012) Interactive hyperspectral approach for exploring and interpreting DESI-MS images of cancerous and normal tissue sections. *Analyst (Lond)* 137(10):2374–2380.
24. James G, Witten D, Hastie T, Tibshirani R (2013) *An Introduction to Statistical Learning: With Applications in R* (Springer, New York).
25. Kiebish MA, Han X, Cheng H, Chuang JH, Seyfried TN (2008) Cardiolipin and electron transport chain abnormalities in mouse brain tumor mitochondria: Lipidomic evidence supporting the Warburg theory of cancer. *J Lipid Res* 49(12):2545–2556.
26. Hsu FF, Turk J (2001) Studies on phosphatidylglycerol with triple quadrupole tandem mass spectrometry with electrospray ionization: Fragmentation processes and structural characterization. *J Am Soc Mass Spectrom* 12(9):1036–1043.
27. Hsu FF, Turk J (2005) Studies on phosphatidylserine by tandem quadrupole and multiple stage quadrupole ion-trap mass spectrometry with electrospray ionization: Structural characterization and the fragmentation processes. *J Am Soc Mass Spectrom* 16(9):1510–1522.
28. Hsu FF, Turk J (2009) Electrospray ionization with low-energy collisionally activated dissociation tandem mass spectrometry of glycerophospholipids: Mechanisms of fragmentation and structural characterization. *J Chromatogr B Analyt Technol Biomed Life Sci* 877(26):2673–2695.
29. Rimmerman N, et al. (2008) N-palmitoyl glycine, a novel endogenous lipid that acts as a modulator of calcium influx and nitric oxide production in sensory neurons. *Mol Pharmacol* 74(1):213–224.
30. Utsugi T, Schroit AJ, Connor J, Bucana CD, Fidler IJ (1991) Elevated expression of phosphatidylserine in the outer membrane leaflet of human tumor cells and recognition by activated human blood monocytes. *Cancer Res* 51(11):3062–3066.
31. Dobrzyńska I, Szachowicz-Petelska B, Sulkowski S, Figaszewski Z (2005) Changes in electric charge and phospholipids composition in human colorectal cancer cells. *Mol Cell Biochem* 276(1-2):113–119.
32. Sarela AI, et al. (2005) Diagnostic variation and outcome for high-grade gastric epithelial dysplasia. *Arch Surg* 140(7):644–649.
33. Friedman J, Hastie T, Tibshirani R (2013) *Glmnet: Lasso and Elastic-Net Regularized Generalized Linear Models*. Available at http://cran.r-project.org/web/packages/glmnet/index.html.